

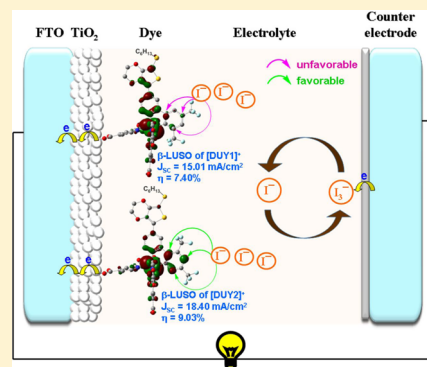
Effect of the CF₃ Substituents on the Charge-Transfer Kinetics of High-Efficiency Cyclometalated Ruthenium Sensitizers

The-Duy Nguyen, Chun-Han Lin, and Chun-Guey Wu*

Department of Chemistry and Research Center for New Generation Photovoltaics, National Central University, Jhong-Li 32001, Taiwan, Republic of China

Supporting Information

ABSTRACT: Six thiocyanate-free complexes, DUY1–DUY6, were synthesized, and their application in a dye-sensitized solar cell was studied to explore the effect of the CF₃ substituent positioned in the ancillary ligand and the structure of the anchoring ligand on the physicochemical properties, charge-transfer kinetics, and photovoltaic properties of ruthenium sensitizers. When the electron-withdrawing groups were installed on the cyclometalating ligands and their π conjugation of the ancillary ligand was extended, the frontier orbital energy levels of the ruthenium complex appeared to be sufficient for effective electron injection and dye regeneration, at the same time having high light-harvesting ability. Two electron-withdrawing CF₃ groups meta to the cyclometalated position reduce the electron density at the metal center less seriously than *o*-CF₃ and *p*-CF₃ groups. The sensitizers containing a *m*-CF₃ group also reveal a more favorable distribution of β lowest unoccupied spin orbital for interaction between the oxidized dyes and the iodide ion, which promotes dye regeneration. The absorption profiles of DUY1–DUY4 adsorbed a TiO₂ film extended to longer wavelength compared to those in an *N,N*-dimethylformamide solution, especially DUY1 and DUY2 dyes, which have λ_{max} red shifts of up to 30 nm. The DUY2-dyed cell exhibited the highest efficiency of 9.03%, while the power conversion efficiencies of DUY1-, DUY3-, DUY4-, and N719-based devices were 7.40%, 7.01%, 8.92%, and 8.63%, respectively. DUY5 and DUY6 (the side products of DUY3 and DUY4) without anchoring groups have very weak physical adsorption on a TiO₂ anode. The corresponding cells exhibit very low efficiency (<0.1%), although both dyes have high light-harvesting ability and proper frontier orbital energy levels.



INTRODUCTION

A dye-sensitized solar cell (DSC), first reported by O'Regan and Grätzel in 1991, is one of the most promising photovoltaic technologies by virtue of its semitransparency, flexibility, impressive photon-to-current conversion efficiency, noteworthy stability, and low manufacturing cost. The device color can also be varied by selecting dyes that absorb at various wavelengths, which enhances the application versatility, such as those used in indoor lighting.¹ To obtain a high conversion efficiency, optimization of the open-circuit potential (V_{OC}) and short-circuit current density (J_{SC}) of the cell is essential. The value of V_{OC} depends on the edge of the TiO₂ conduction band known to have a Nernstian dependence on the pH value² and the redox potential of the mediator. Meanwhile, J_{SC} is related to the light-harvesting properties of the sensitizer, the interaction between the sensitizer and TiO₂ anode, and the charge-transfer processes in the device. Both optical and electronic properties of the complex sensitizers can be tuned in two ways: by the introduction of a ligand with a low-lying π^* molecular orbital or by destabilization of the metal t_{2g} orbital through the introduction of a strong donor ligand. The former lowers the energy of the lowest unoccupied molecular orbital (LUMO), while the latter destabilizes the highest occupied molecular orbital (HOMO) of the sensitizer, ultimately decreasing the

HOMO–LUMO energy gap (E_{gap}).³ Another method to red-shift the absorption and enhance the molar absorption coefficient of the sensitizer is to extend the π -conjugation length of the ancillary and/or anchoring ligands.^{1,4–6} Nevertheless, this method sometimes exhibits a trade-off of J_{SC} and V_{OC} due to the fast charge recombination at the TiO₂/electrolyte interface caused by the poor TiO₂ surface protection of the bulky sensitizers with big ancillary ligands.⁷

One of the most successful sensitizers is N719 ($J_{\text{SC}} = 17.73$ mA/cm², $V_{\text{OC}} = 846$ mV, FF = 0.75, and $\eta = 11.18\%$).⁸ However, the main drawbacks of N719 are the lack of absorption in the red region of the visible spectrum³ and the presence of monodentate thiocyanate (NCS) ligands. Although the NCS ligand can encourage dye regeneration by interacting with I⁻ and red-shifting the absorption profile by destabilizing the HOMO, it is a monodentate ligand, which makes replacement by other ligands (such as *N,N*-dimethylformamide, acetonitrile, 3-methoxypropionitrile, and 4-*tert*-butylpyridine) possible, resulting in low cell stability under excessive thermal stress and/or light soaking.^{9–12} Furthermore, because of its structure and ambidentate nature, the NCS ligand is difficult to

Received: August 29, 2016

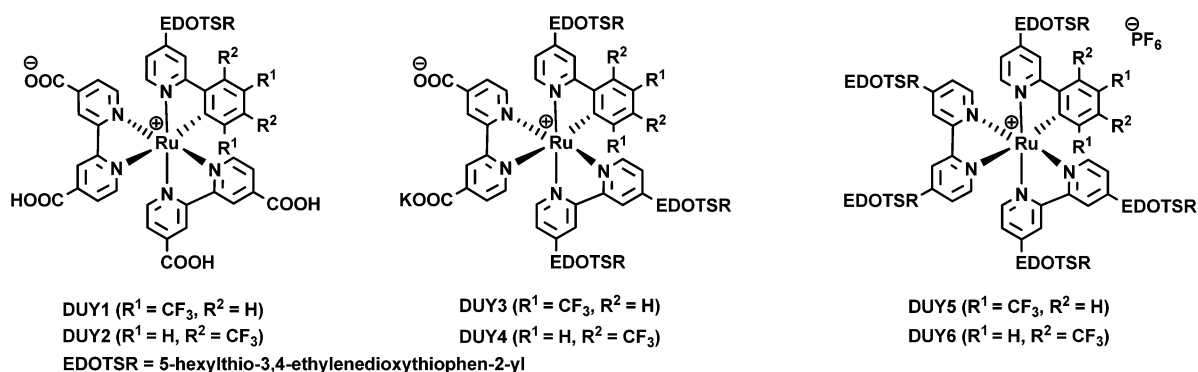


Figure 1. Structures of DUY series sensitizers.

modify and dye purification steps are virtually required to separate the active N-coordinated isomer from the inactive S-coordinated isomer.¹² One of the common approaches for replacing NCS ligands is using cyclometalating bidentate ligands^{5,12–18} that can manipulate the electronic and optical properties of the sensitizer by modifying the substituents on the ligand. However, a ruthenium complex containing a cyclometalating ligand generally has a high HOMO level, which may decrease the driving force for dye regeneration.^{5,16–18} Adding an electron-withdrawing group (such as CF_3) on the cyclometalating ligand is a strategy to lower the HOMO level to facilitate dye regeneration. In this paper, we reported the physicochemical and photovoltaic properties of four high-efficiency NCS-free, CF_3 -substituted cyclometalated ruthenium complexes (DUY1–DUY4) and two model complexes (DUY5 and DUY6). Their structures are displayed in Figure 1. This study mainly focuses on the effects of the CF_3 -substituent positions on the charge-transfer kinetics and the photovoltaic performance of the ruthenium dyes. The ultimate purpose is to understand the structure–property relationship of a ruthenium complex containing a CF_3 -substituted cyclometalated ancillary ligand in order to develop NCS-free high-efficiency cyclometalated complex sensitizers for DSC.

EXPERIMENTAL SECTION

Materials and Measurements. All reagents were obtained from commercial sources and used as received unless specified. Solvents were dried over 4 Å molecular sieves or CaH_2 before use. The detail preparation and structure characterization steps of the six ruthenium complexes are collected in the Supporting Information (SI). NMR spectra were recorded on a Bruker 300 MHz NMR spectrometer. High-resolution mass spectrometry (HRMS) spectra were obtained using a JMS-700 HRMS spectrometer. Elemental analyses were carried out with a PerkinElmer 2400 CHNS/O analyzer. UV–vis spectra of the dyes in *N,N*-dimethylformamide (DMF) and adsorbed on a TiO_2 film were measured using a Cary 300 Bio spectrometer. Voltammetric measurements were performed in a single-compartment, three-electrode cell with a platinum wire counter electrode and a platinum disk working electrode. The reference electrode was Ag^+/Ag , and the supporting electrolyte was 0.1 M tetrabutylammonium perchlorate in DMF. The square-wave voltammograms of the sensitizers dissolved in DMF (potential step increment = 5 mV; frequency = 25 Hz) were recorded using a potentiostat/galvanostat (PGSTAT30, Eco-Chemie Autolab, Utrecht, The Netherlands), and ferrocene was used as a calibration internal standard. Electrochemical impedance spectroscopy (EIS) measurements were carried out using an Eco Chemie Autolab PGSTAT30 potentiostat/galvanostat in 50 mV voltage steps with a sinusoidal potential perturbation of 10 mV in the dark. Intensity-modulated photocurrent spectroscopy (IMPS) and intensity-modulated photovoltage spectroscopy (IMVS) were recorded with a Zahner

Zennium CIMPS-1 potentiostat installed with a light-intensity-modulated function to control the light intensity. Transient absorption spectroscopy (TAS) measurements were performed on a Proteus Ultrafast System with a custom-designed light path. The measurements (EIS, IMPS, IMVS, and TAS) and relative calculations can be found in our previous papers.^{6,19}

Density Functional Theory (DFT) Calculation. DFT calculations were performed using the Gaussian 09 program.²⁰ For ground-state geometry optimization, the B3LYP (Becke, three-parameter, Lee–Yang–Parr) hybrid functional^{21,22} was used. The LanL2DZ effective core potential²³ was used for the ruthenium atom, and the split-valence 6-31G(d,p) basis set²⁴ was applied for the hydrogen, sulfur, carbon, oxygen, nitrogen, and fluorine atoms. The time-dependent DFT (TD-DFT) excited-state calculation of the lowest singlet–singlet electronic transitions was also performed using the same basic sets. The solvent effects were included in the calculations using the conductor-like polarizable continuum model.^{25–27}

Device Fabrication and Photovoltaic Performance Characterization. The preparation of TiO_2 pastes, fabrication of a TiO_2 anode, dye loading, assembly, and photovoltaic parameter measurements of the cells were similar to what we reported previously⁶ unless specified.

RESULTS AND DISCUSSION

Strategy for the Design of the Sensitizers. DUY1 and DUY2 were derived from the replacement of two NCS ligands in N719 with cyclometalating bidentate ligands named 2-[3,5-bis(trifluoromethyl)phenyl]-4-[5-(hexylthio)-3,4-ethylenedioxythiophenyl]pyridine (LD1) and 2-[2,4-bis(trifluoromethyl)phenyl]-4-[5-(hexylthio)-3,4-ethylenedioxythiophenyl]pyridine (LD2), respectively. The electron-donating character of the negatively charged 2-phenylpyridine (ppy^-) unit could destabilize the HOMO levels, reduce the HOMO–LUMO energy gap, and bathochromically shift the absorption profile, especially the metal-to-ligand charge-transfer transitions. To maintain a sufficient driving force for dye regeneration (lowering of the HOMO level), two electron-withdrawing CF_3 substituents were introduced to the benzene ring of the cyclometalated ligand. Depending on the spatial closeness of the CF_3 substituents to the cyclometalated position, the *o*- and *p*- CF_3 substituents of DUY1 were expected to show a stronger influence on the HOMO level of the dye compared to the two *m*- CF_3 substituents for DUY2. DUY3 and DUY4 were designed by extending the π -conjugation systems with the 5-(hexylthio)-3,4-ethylenedioxythiophen-2-yl (EDOTSHexyl) moiety attached on one of the anchoring ligands of DUY1 and DUY2, respectively. The functions of EDOTSHexyl not only improve the absorption of the dye and suppress dye aggregation but also keep the hydrophilic water from approaching the TiO_2 surface.

DUY5 and DUY6, the side products of DUY3 and DUY4, respectively, were used as model compounds to further confirm the effects of the CF₃-substituent positions on the photo-physical and electrochemical properties of a ruthenium sensitizer. They were also used to reveal the adsorption behavior (on TiO₂) and photovoltaic performance of sensitizers having all ligands without a carboxylate group but with a CF₃-substituted cyclometalated ligand.

Synthesis and Characterization. For the preparation of ligands LD1 and LD2, we chose 2-bromo-4-aminopyridine as the starting material. Compared to the use of 2-bromo-4-iodopyridine for the synthesis of 4-substituted ppy⁻,²⁸ 2-bromo-4-aminopyridine exhibited some advantages, such as low cost, stability at ambient temperature, insensitivity to moisture or light, ease of handling, a few side products after coupling reactions (because there are no competitive reactions), and short purification time. Six complexes, DUY1–DUY6, were prepared by modifying procedures developed by Berlinguette and co-workers.^{13,14} The addition of C[^]N (C[^]N = bidentate cyclometalating ligand, e.g., ligands LD1 and LD2) to [(η⁶-*p*-cymene)RuCl₂]₂ at 45 °C led to both [Ru(CH₃CN)₄(C[^]N)]PF₆ and [Ru(*p*-cymene)(CH₃CN)₂(C[^]N)]PF₆ in approximate equimolar amounts. Only [Ru(CH₃CN)₄(C[^]N)]PF₆ is a useful precursor for the later syntheses because [Ru(*p*-cymene)(CH₃CN)₂(C[^]N)]PF₆ does not react with 2,2'-bipyridyl-4,4'-dicarboxylic acid to an appreciable extent.¹⁵ We note that [Ru(CH₃CN)₄(C[^]N)]PF₆ is the main product at 55 °C because [Ru(*p*-cymene)(CH₃CN)₂(C[^]N)]PF₆ can convert to [Ru(CH₃CN)₄(C[^]N)]PF₆ at either higher temperature or longer reaction time.¹⁴

The solubility of DUY1–DUY6 in organic solvents (e.g., CH₂Cl₂, CHCl₃, CH₃OH, CH₃CN, and DMF) follows the order of DUY1 < DUY2 ≪ DUY3 ≈ DUY4 < DUY5 ≈ DUY6, indicating that their solubility is determined by the number of alkyl chains. Therefore, DUY3–DUY6 could be simply purified by conventional silica gel chromatography, while DUY1 and DUY2 needed to be isolated by reversed-phase chromatography after dissolution in a 0.2 M tetrabutylammonium/methanol solution. NMR data indicated that all complexes exist as a single isomer with structures displayed in Figure 1.²⁹ DUY3 and DUY4 could have the Ru–C bond trans to either 2,2'-bipyridine-4,4'-dicarboxylate or 4,4'-bis[5-(hexylthio)-3,4-ethylenedioxythiophenyl]-2,2'-bipyridine (ligand B20). The resulting configurations of DUY3 and DUY4 could be expected by the trans effect and the reactivity of the ligands in the coordination reaction. Et₂dcbpy has a smaller molecular size and could make a stronger synergistic bonding with the ruthenium metal center than ligand B20,¹⁵ while the negatively charged carbon atom of the cyclometalating ligand induced a higher trans effect of the benzene ring compared to the pyridine ring.³⁰ As a consequence, the first step of the coordination reaction is the replacement of two CH₃CN molecules in [Ru(CH₃CN)₄(C[^]N)]PF₆ (one trans to the benzene ring and one cis to both the benzene ring and the pyridine ring of the cyclometalating ligand) with Et₂dcbpy, and in the next step, the remaining acetonitrile ligands were replaced with ligand B20 to produce the ester form of DUY3 or DUY4. After hydrolysis, DUY3 and DUY4 were obtained with the conformation shown in Figure 1. The chemical shifts of the ortho protons in the benzene ring of DUY4 and its ester form are almost the same (Δδ = 0.013 ppm), also indicating that Et₂dcbpy oriented trans to the benzene ring and evidently the ligand B20 trans to the pyridine ring of the cyclometalating ligand.³¹ These results are

consistent with the studies by Berlinguette and co-workers¹⁶ as well as Frey and co-workers,¹⁷ who proved that the configuration of tris-heteroleptic cycloruthenated dyes had the cyclometalating ring positioned trans to 2,2'-bipyridine-4,4'-dicarboxylate based on the X-ray diffraction data.

Optical Properties. The absorption spectra of DUY sensitizers and N719 dissolved in DMF solutions and adsorbed on thin TiO₂ films are depicted in Figure 2. All sensitizers (in

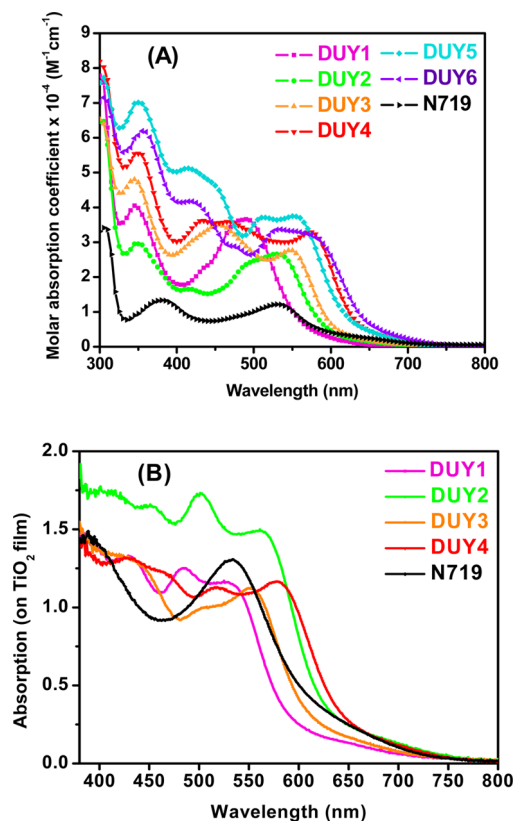


Figure 2. (A) Absorption spectra of the DUY sensitizers and N719 dissolved in DMF and (B) absorption spectra of DUY1–DUY4 and N719 anchored on transparent TiO₂ films.

DMF) show a strong absorption band around 350 nm with a molar absorption coefficient (ϵ) in the range of $(3.0\text{--}7.0) \times 10^4 \text{ M}^{-1} \text{ cm}^{-1}$ assigned to the $\pi\text{--}\pi^*$ transitions of the cyclometalated ligands. A series of broad absorption bands at longer wavelength are primarily from the mixed-metal/ligand-to-ligand charge-transfer (MMLLCT) transitions.^{14,17} The extinction coefficients of the DUY sensitizers are all remarkably higher than that of N719 in the whole absorption range. The absorption maxima (λ_{max}) of the lowest-energy band of the sensitizers are in the order of DUY1 < DUY2 < N719 < DUY3 < DUY5 < DUY4 < DUY6. The electron-withdrawing nature of the CF₃ groups on the cyclometalating ligands makes λ_{max} of DUY1 and DUY2 shorter than that of N719. On the contrary, DUY3–DUY6 sensitizers show a red shift in λ_{max} compared to N719 due to the presence of the electron-donating ancillary ligand B20 on the DUY dyes.

Electrochemical Properties. The HOMO energy levels of the DUY sensitizers were determined with square-wave voltammetry, as shown in Figure 3A. The only oxidation peak of the DUY1 and DUY2 dyes is assigned to the oxidation of Ru^{II} to Ru^{III}.¹⁷ DUY3–DUY6 exhibit an extra three-electron oxidation peak at $\sim 1.47 \text{ V}$ vs NHE, which is assigned to the

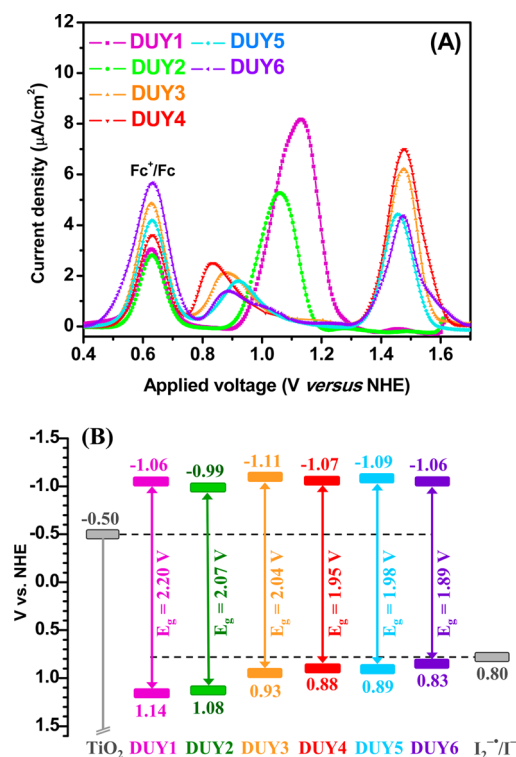


Figure 3. (A) Square-wave voltammograms and (B) frontier orbital energy-level diagram of DUY sensitizers.

oxidation of 4-[5-(hexylthio)-3,4-ethylenedioxythiophenyl]pyridin-2-yl units. The positions of the electron-withdrawing CF₃ groups on the cyclometalating ligand can give rise to distinct impacts on the oxidation potentials of the sensitizers. Two CF₃ groups at ortho and para positions reduce the electron density at the metal center more efficiently than two *m*-CF₃ groups. As a consequence, DUY1, DUY3, and DUY5 have HOMO levels 50–60 mV more positive than those of DUY2, DUY4, and DUY6, respectively (see Figure 3A). Ligand B20 is a strong donor that also plays a role in the tuning of the HOMO levels of the sensitizers. Replacement of a bipyridinedicarboxylic acid ligand with a ligand B20 leads to a 200–210 mV rise in the HOMO level (such as DUY3 and DUY4), while a 250 mV rise was obtained by substituting two bipyridinedicarboxylic acids with two B20 ligands (such as DUY5 and DUY6). The ground-state energy levels of the DUY sensitizers are in a range of 0.83–1.14 V, which are all more positive than the threshold (~0.8 V vs NHE) for dye regeneration by I⁻ in the redox couple.^{18,32} The LUMO energy levels (E_{LUMO}) of the dyes were calculated by the formula $E_{\text{LUMO}} = E_{\text{HOMO}} - E_{\text{gap}}$, where E_{gap} values are obtained from the onset of their absorption spectra illustrated in Figure 2A. The HOMO and LUMO energy levels of all DUY dyes are summarized in Figure 3B. The LUMO levels of all sensitizers are found to be at least 490 mV higher than the Fermi level of the TiO₂ film,¹⁵ providing a sufficient driving force for electron injection. The energy levels of the frontier orbitals suggest that DUY1–DUY6 are all appropriate dyes for application in DSCs.² Furthermore, the σ -donating ligands (LD1, LD2, and B20) affect HOMOs more than LUMOs by transferring the electron density to the metal center.⁵ In this sense, E_{gap} values also depend on the positions of the electron-withdrawing CF₃ groups on the cyclometalating ligands and the number of ligand B20 in the complexes. As a result, the energy gaps of the DUY

sensitizers are in the order of DUY1 > DUY2 > DUY3 > DUY5 > DUY4 > DUY6.

The electronic absorption spectra of DUY1–DUY4 and N719 immobilized on the transparent TiO₂ films displayed in Figure 2B show a red shift of λ_{max} (especially those for DUY1 and DUY2, which red-shift about 30 nm) along with a change in the absorption profile compared to those in DMF. This is probably because of the increasing electronic coupling between the π and π^* orbitals of the ancillary ligands.³³ The spectra of the DUY5 and DUY6 sensitizers have not been shown here because they almost cannot anchor on the TiO₂ surface. The absorption profiles of DUY dyes adsorbed on TiO₂ films are also wider compared to those for the dyes in DMF. The widening of the absorption profile is reasonably attributed to the dye molecules with various conformations coexisting on the TiO₂ surface, due to the bulky nature of NCS-free ruthenium complexes.⁶ This probably is one of the benefits for designing a sensitizer with bulky ancillary ligand/structure. Furthermore, compared to the absorption of N719 on a TiO₂ thin film, the absorption profiles shown in Figure 2B clearly reveal that DUY2 and DUY4 are able to absorb more light than N719 when applied in DSC devices.

Theoretical Calculation of the Frontier Molecular Orbital Distributions and Electronic Transitions. The graphical representation of the computational frontier orbital distribution is illustrated in Figures S1–S6 (see the SI). The HOMOs of all DUY1–DUY6 are contributed primarily from both the metal and ligands (cyclometalating and/or polypyridyl ligands), while the LUMOs virtually distribute on the polypyridyl (anchoring) ligands, suggesting that the broad absorption bands of the sensitizers result predominantly from the MMLLCT transitions.¹⁴ The partial contribution of ppy⁻ and/or 4-[5-(hexylthio)-3,4-ethylenedioxythiophenyl]pyridin-2-yl units to the HOMOs indicates that the cyclometalating ligands and ligand B20 could influence localization of the HOMO levels. On the other hand, because the LUMOs virtually distribute on the polypyridyl ligands, cyclometalation of the metal center does not destabilize the LUMOs. Empty molecular orbitals (see Figures S1 and S2 in the SI) of DUY1 and DUY2 are almost all localized on the anchoring ligands, while for DUY3 and DUY4, the empty molecular orbitals (see Figures S3 and S4 in the SI) are virtually contributed from the 4-[5-(hexylthio)-3,4-ethylenedioxythiophenyl]pyridin-2-yl units. For this reason, both DUY1 and DUY2 may exhibit higher electron injection efficiency than DUY3 and DUY4 (from the photoexcited dyes to the conduction band of TiO₂).

To gain more insight into the absorption bands, TD-DFT calculation of the singlet electronic transition was performed using DMF as the solvent. The calculated oscillator strengths and electron density difference maps as well as the experimental absorption spectra for DUY dyes are displayed in Figures S7–S12 in the SI, and the detailed transition assignments are listed in Tables S1–S6 in the SI. The calculated oscillator strengths are quite close to the experimental absorption spectra, although the calculated λ_{max} values are blue-shifted compared to the experimental data for all dyes. The results imply that variation in the electronic properties of these types of sensitizers could be predicted by a routine theoretical calculation. DUY1 and DUY2 have six (S_5 , S_6 , S_7 , S_{11} , S_{13} , and S_{16}) and five (S_7 , S_8 , S_{10} , S_{11} , and S_{16}), respectively, strong transitions with oscillator strengths (f) > 0.1 (see Tables S1 and S2 in the SI). These transitions are believed to contribute significantly to the photocurrent because photoexcited electrons could be

effectively injected into the conduction band of TiO₂ from these transitions through the anchoring ligands on which the empty molecular orbitals located. On the contrary, the transition assignments of DUY3 and DUY4 (see Tables S3 and S4 in the SI) indicate that the electron injection corresponding to the strong transitions is less efficient because some of the empty molecular orbitals locate on 4-[5-(hexylthio)-3,4-ethylenedioxythiophenyl]pyridin-2-yl units instead of on the anchoring ligand. On the basis of the estimated electron injection and optical data without considering the dye loading, we may expect that J_{SC} of the corresponding cell is in the order of DUY1 > DUY2 > DUY4 > DUY3.

Photovoltaic Performance. The J - V and IPCE curves for DUY1–DUY4-sensitized devices are displayed in Figure 4. The

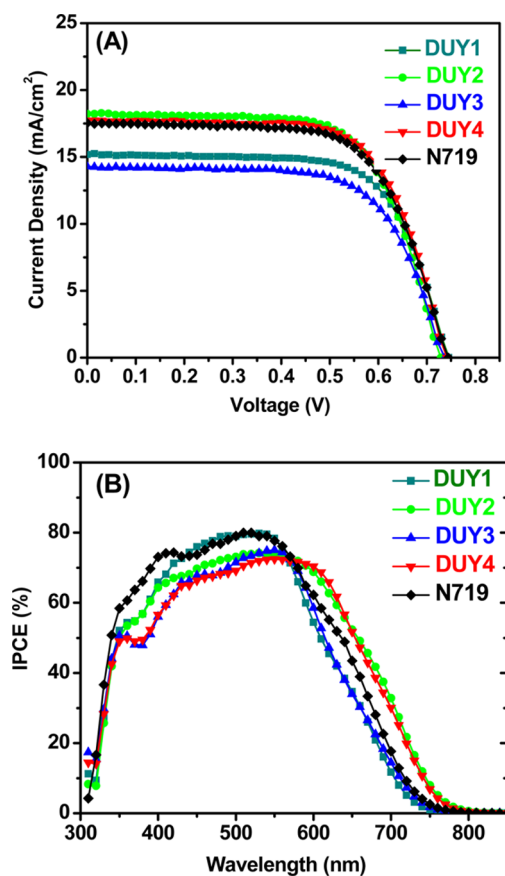


Figure 4. (A) J - V and (B) IPCE curves of DUY1–DUY4- and N719-sensitized devices.

photovoltaic parameters and dye loading (also including those of N719, DUY5, and DUY6) are summarized in Table 1. Under

the illumination of AM 1.5 G simulated sunlight, the power conversion efficiencies of DUY5- and DUY6-based cells are very low because very few dye molecules could adsorb on TiO₂ (DUY5- and DUY6-adsorbed TiO₂ anodes look white). These results indicate that the weakly physical interaction between the dye (without a carboxylate group) and TiO₂ is not sufficient for adsorbing the sensitizer on the TiO₂ surface. It seems that even the few DUY5 and DUY6 impurities existing in DUY3 and DUY4 may not significantly affect the photovoltaic performance of DUY3 and DUY4 when applied in DSC. DUY1–DUY4-based cells exhibit efficiencies of 7.40%, 9.03%, 7.01%, and 8.92%, respectively, while that of the N719-based cell is 8.63%. Like the absorption spectra displayed in Figure 2B, the high efficiency of DUY2 and DUY4 could be derived from the strongest absorption of DUY2 and the widest absorption range of DUY4 when they adsorbed on a TiO₂ film. Interestingly, DUY2- and DUY4-based cells display higher IPCE values at 590–800 nm than DUY1- and DUY3-sensitized cells because the DUY2- and DUY4-dyed TiO₂ films have a stronger absorption at long wavelength (see Figure 2B). Data listed in Table 1 show that V_{OC} and FF of all cells are very close to each other. As a consequence, the efficiency of the cell is mainly determined by J_{SC} . The order of the dye loadings (DUY2 > DUY4 > DUY3 > DUY1; see Table 1) implies that the positions of the CF₃ groups on the cyclometalating ligand affect the dye loading like the bulk ancillary ligand B20 does. DUY2 has the highest dye loading among all of the sensitizers because of its small molecular size; therefore, the corresponding cell achieves the highest J_{SC} . The lowest dye loading of DUY1 could originate from its poor solubility in organic solvents used for dissolving dye. Nevertheless, J_{SC} of a DUY1-sensitized device is higher than that of a cell based on DUY3 because DUY1 has a stronger absorption at 450–525 nm [in this range, the standard sunlight (AM 1.5 G) has the largest photo number] than DUY3 (see Figure 2). Furthermore, the driving force for dye regeneration of DUY1 is higher than that of DUY3 because the former has a lower HOMO level (see Figure 3B).

Charge-Transfer Kinetics inside the Cells. To obtain the dynamics of the interfacial charge-transfer processes within the devices, EIS, IMPS/IMVS, and TAS spectra were employed to estimate the resistance at the TiO₂/dye/electrolyte interface, the transport time (τ_{tr}) and lifetime (τ_n) of the electron on TiO₂, as well as the dye regeneration kinetics, respectively. EIS spectra (Nyquist plots) of the devices taken under illumination and in the dark are illustrated in Figure 5. The second semicircle of the EIS Nyquist plot taken in the dark typically presents to the interfacial resistance (R_2) of TiO₂/dye/electrolyte interfaces.³⁴ At the illumination and open-circuit conditions, the charge-transfer processes at the interface are composed of electron injection from the light-excited dye to the

Table 1. Photovoltaic Parameters, Dye Loading, TiO₂/Dye/Electrolyte Interface Resistance (R_2), and Regeneration Times of the Sensitizers

dye	J_{SC} (mA/cm ²)	V_{OC} (V)	FF	η (%)	dye loading ($\times 10^{-7}$ mol/cm ²)	R_2 (Ω , illum)	R_2 (Ω , dark)	τ_1 (μ s)	τ_2 (μ s)
DUY1	15.01	0.733	0.67	7.40	4.96	19.9	100	7.47	402.1
DUY2	18.40	0.737	0.67	9.03	5.85	17.2	104	6.63	378.4
DUY3	14.29	0.737	0.67	7.01	5.08	22.6	104	11.8	385.2
DUY4	17.74	0.741	0.68	8.92	5.29	18.9	110	7.59	383.1
DUY5	0.13	0.391	0.42	0.02					
DUY6	0.13	0.381	0.42	0.02					
N719	17.54	0.744	0.66	8.63					

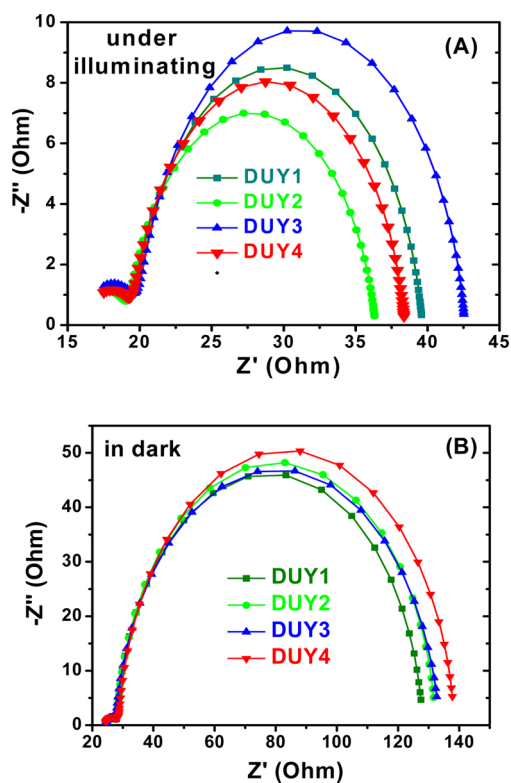


Figure 5. EIS spectra (Nyquist plots) of DUY-sensitized cells: (A) under AM 1.5 G illumination; (B) in the dark.

TiO₂ conduction band, the charge recombination of electrons from the TiO₂ conduction band to the oxidized dye, and the oxidizing component in the redox couple. The R2 values calculated from the EIS spectra are also listed in Table 1. Under illumination, the DUY2-dyed cell has the smallest R2, indicating that the cell possesses the most facile electron-transport cycle and therefore exhibits the largest J_{SC} . The order of the R2 values (DUY3 > DUY1 > DUY4 > DUY2) indicated that both the dye loading and driving force of dye regeneration are important parameters for determining the R2 value under illumination. Higher dye loading and dye regeneration driving force result in a smaller R2 value. On the other hand, in the dark conditions, the R2 values for all cells are very similar and much larger than the R2 values under illumination, suggesting that there is no big difference in the charge recombination of all DUY-sensitized cells; therefore, the V_{OC} values for all cells are also very close (see Table 1).

Figure 6 displays the electron-transport time (τ_{tr}) and electron lifetime (τ_n , also called recombination time) of cells obtained from the IMPS and IMVS data. τ_{tr} and τ_n represent the time that the electrons on TiO₂ transit across to the photoanode and recombine with I₃⁻ in the electrolyte, respectively. For a good performance cell, the electron-transport time should be shorter than the electron lifetime.³⁵ τ_{tr} values for all devices studied are much smaller than τ_n values, suggesting that all cells could have high efficiencies. τ_{tr} is in the ascending order of DUY2 < DUY4 < DUY1 < DUY3 (see Figure 6A), which is consistent with the J_{SC} order (DUY2 > DUY4 > DUY1 > DUY3; see Table 1). Like the data shown in Figure 6B, at low light intensity, the DUY4-sensitized cell has the highest τ_n value. Nevertheless, when the light intensity increases, the τ_n values of all cells tend to be very close. The V_{OC} values of all cells (see Table 1) are very close because the

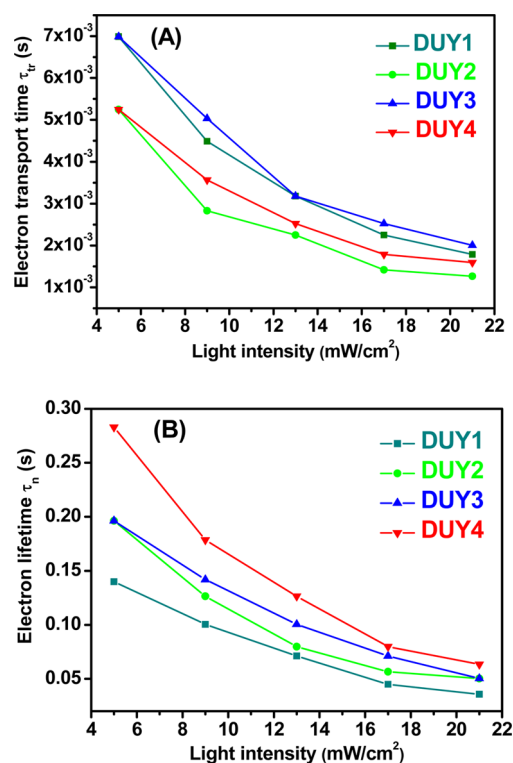


Figure 6. (A) Electron-transport time and (B) electron lifetime as a function of the light intensity for DSCs based on DUY1–DUY4.

V_{OC} values of all cells were measured at a light intensity (100 mW/cm²) much stronger than those (5–22 mW/cm²) used in the IMPS and IMVS studies. The results of both the interfacial resistance (from EIS in the dark) and electron lifetime (from IMVS) support the analogous charge recombination of DUY1–DUY4-sensitized cells, even though the dye loading of DUY1 is significantly lower than that of DUY2.

The kinetics of dye regeneration can be derived from the TAS spectra of the cells illustrated in Figure S13 in the SI. Two regeneration times, τ_1 and τ_2 , corresponding to the reduction of the oxidized dye by the electrolyte and by the electron on TiO₂, respectively,⁶ are also listed in Table 1. For all devices, τ_1 is much smaller than τ_2 , which means that reduction of the oxidized dye by iodide in the electrolyte is the major process for dye regeneration. The regeneration time is usually related to the HOMO level of the dye molecule: the lower the HOMO level, the shorter the regeneration time.⁶ This tendency was distinctly observed when the HOMO levels and τ_1 values of sensitizers possessing the same CF₃ positions (such as the DUY1/DUY3 pair or the DUY2/DUY4 pair) were compared. Nevertheless, the trend of τ_1 was not consistent with the order of the HOMO levels for sensitizers having different CF₃ positions (like the DUY1/DUY2 pair or the DUY3/DUY4 pair). This phenomenon indicates that the kinetics of dye regeneration also depends on other factors (such as the positions of the CF₃ groups on the cyclometalating ligands) besides the HOMO levels. In the working condition of a DSC, the oxidation of a dye would involve the excitation of one electron from the HOMO to the LUMO and then excited electron injection from the LUMO to the TiO₂ conduction band edge. After electron injection, the HOMO of the dye becomes a single occupied molecular orbital (SOMO), which involves an α highest occupied spin orbital (α -HOSO) and a β lowest unoccupied spin orbital (β -LUSO).^{36,37} The calculated

β -LUSO of the oxidized DUY sensitizers, displayed in Figure 7, shows the most orbital character on the ruthenium centers and

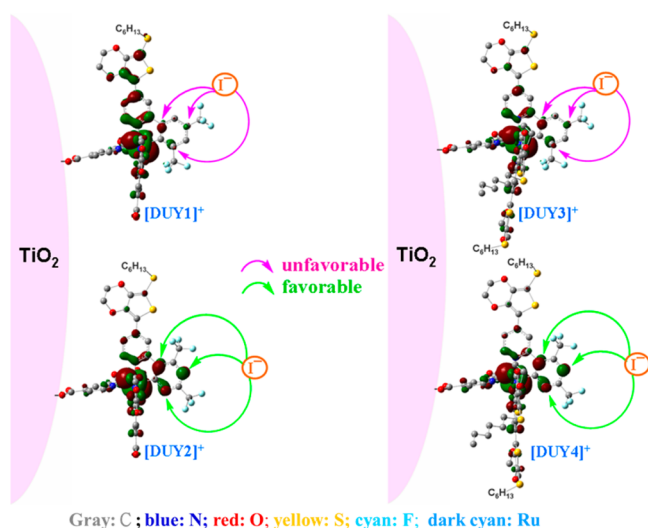


Figure 7. DFT models of the oxidized DUY1–DUY4 sensitizers, along with their β -LUSO distributions and the proposed approaches of I^- to the oxidized dyes.

some on the cyclometalated ligand, indicating that the positive charge of the dye cations is more localized on the ruthenium. Dye regeneration corresponds to the transfer of one electron from the iodide ion to the β -LUSO of the oxidized dye, and the more widely distributed β -LUSO will result in better interaction between the oxidized dye and the iodide ion. Nevertheless, once dye regeneration occurs through direct Ru–I interaction, a seven-coordination Ru^{3+} complex (which appears not to exist in the literature) will form.³⁸ Additionally, all attempts by Privalov and co-workers had failed to computationally optimize a seven-coordinated structure of a Ru^{III} complex.⁹ Therefore, instead of direct Ru–I interaction, we consider that dye regeneration should take place at other atoms that contribute to the β -LUSO such as the cyclometalated ancillary ligand. After carefully considering the relationship of the dye regeneration time (Table 1) and the β -LUSO distribution on cyclometalating ligands (Figure 7), we believe that the dye regeneration time is strongly influenced by the β -LUSO contribution from the 2,4-bis(trifluoromethyl)phenyl unit more than that from the EDOTSHexyl unit because the hexyl chain can prevent the approach of the iodide ion. At the same isovalue = 0.02 (Figure 7), [DUY2]⁺ and [DUY4]⁺ possess a larger β -LUSO character on the 2,4-bis(trifluoromethyl)phenyl ring than [DUY1]⁺ and [DUY3]⁺, respectively. Furthermore, the calculated β -LUSOs displayed in Figure 7 reveal that the β -LUSO of the all oxidized dye ([DUY]⁺) is distributed more on the *o*- and *p*-carbon atoms compared to the aromatic *m*-carbon atoms on the cyclometalating ligand. The *m*-CF₃ substituents of [DUY2]⁺ and [DUY4]⁺ are more favorable for approaching of the iodide ion because of the less spatial hindrance of the substituents. Consequently, DUY2- and DUY4-based cells exhibit faster dye regeneration and larger J_{SC} than the DUY1- and DUY3-based cells, respectively.

CONCLUSION

In summary, six NCS-free cyclometalated ruthenium complexes were synthesized and examined in the context of structure–property (including the photovoltaic performance) relationships. The trans effect and ¹H NMR spectra were successfully used to define the configurations of the heteroleptic octahedral complexes DUY3 and DUY4 to be the cyclometalating ring positioned trans to 2,2'-bipyridine-4,4'-dicarboxylate. The light-harvesting ability can be increased by extending the π conjugation of the ancillary ligands; however, it will raise the HOMO level of the sensitizer. Installing the electron-withdrawing groups on the cyclometalating ligands can lower the HOMO level for effective dye regeneration. The experimental data indicate that two *m*-CF₃ groups on the cyclometalated position reduce the electron density at the metal center less significantly than those at ortho and para positions. The distribution of β -LUSO of the sensitizers reveals that the dye containing two *m*-CF₃ groups on the cyclometalated ligand is more favorable for the interaction between the oxidized dyes and the iodide ion because of less steric hindrance. DUY2 has two CF₃ groups in the meta positions, the low HOMO level and the high dye loading. As a consequence, the corresponding cell exhibited the best efficiency of 9.03%, which is 5% higher than that of a N719-based cell fabricated at the same condition. This study provides a new direction for designing new high-efficiency NCS-free cyclometalated sensitizers for DSC.

ASSOCIATED CONTENT

Supporting Information

The Supporting Information is available free of charge on the ACS Publications website at DOI: 10.1021/acs.inorgchem.6b02088.

Synthesis, ¹H NMR, HRMS, elemental analysis, TD-DFT-calculated absorption, oscillator strengths, orbital transition probabilities of the singlet optical transitions, frontier orbitals of complexes DUY1–DUY6, and TAS spectra of DUY1–DUY4-sensitized devices (PDF)

AUTHOR INFORMATION

Corresponding Author

*E-mail: t610002@cc.ncu.edu.tw (C.-G.W.).

ORCID

Chun-Guey Wu: 0000-0001-8540-5602

Notes

The authors declare no competing financial interest.

ACKNOWLEDGMENTS

Financial support (Grant NSC 104-2113-M-008-002-MY3) from the Ministry of Science and Technology (MOST), Taiwan, is gratefully acknowledged. The device fabrications and photovoltaic parameter measurements were performed at the Advanced Laboratory of Accommodation and Research for Organic Photovoltaics, MOST, Taiwan, Republic of China.

REFERENCES

- Sridhar, N.; Freeman, D. *26th European Photovoltaic Solar Energy Conference and Exhibition*, Hamburg, Germany, 2011; Fraunhofer-Institut für Solare Energiesysteme ISE: Breisgau, Germany, 2011; pp 232–236.
- Hagfeldt, A.; Boschloo, G.; Sun, L.; Kloo, L.; Pettersson, H. Dye-sensitized solar cells. *Chem. Rev.* **2010**, *110*, 6595–6663.

- (3) Yum, J.-H.; Baranoff, E.; Wenger, S.; Nazeeruddin, M. K.; Grätzel, M. Panchromatic engineering for dye-sensitized solar cells. *Energy Environ. Sci.* **2011**, *4*, 842–857.
- (4) Chen, C.-Y.; Wu, S.-J.; Wu, C.-G.; Chen, J. G.; Ho, K. C. A ruthenium complex with superhigh light-harvesting capacity for dye-sensitized solar cells. *Angew. Chem., Int. Ed.* **2006**, *45*, 5822–5825.
- (5) Hussain, M.; Islam, A.; Bedja, I.; Gupta, R. K.; Han, L.; El-Shafei, A. A comparative study of Ru(II) cyclometallated complexes versus thiocyanated heteroleptic complexes: thermodynamic force for efficient dye regeneration in dye-sensitized solar cells and how low could it be? *Phys. Chem. Chem. Phys.* **2014**, *16*, 14874–14881.
- (6) Li, J. Y.; Lee, C.; Chen, C. Y.; Lee, W. L.; Ma, R.; Wu, C. G. Diastereoisomers of ruthenium dyes with unsymmetric ligands for DSC: Fundamental chemistry and photovoltaic performance. *Inorg. Chem.* **2015**, *54*, 10483–10489.
- (7) Yu, Q.; Liu, S.; Zhang, M.; Cai, N.; Wang, Y.; Wang, P. An extremely high molar extinction coefficient ruthenium sensitizer in dye-sensitized solar cells: The effects of π -conjugation extension. *J. Phys. Chem. C* **2009**, *113*, 14559–14566.
- (8) Nazeeruddin, M. K.; De Angelis, F.; Fantacci, S.; Selloni, A.; Viscardi, G.; Liska, P.; Ito, S.; Takeru, B.; Grätzel, M. Combined experimental and DFT-TDDFT computational study of photoelectrochemical cell ruthenium sensitizers. *J. Am. Chem. Soc.* **2005**, *127*, 16835–16847.
- (9) Privalov, T.; Boschloo, G.; Hagfeldt, A.; Svensson, P. H.; Kloo, L. A study of the interactions between Γ/I_3^- redox mediators and organometallic sensitizing dyes in solar cells. *J. Phys. Chem. C* **2009**, *113*, 783–790.
- (10) Hoggard, P. E.; Porter, G. B. Photoanation of the tris(2,2'-bipyridine)ruthenium(II) cation by thiocyanate. *J. Am. Chem. Soc.* **1978**, *100*, 1457–1463.
- (11) Nguyen, H. T.; Ta, H. M.; Lund, T. Thermal thiocyanate ligand substitution kinetics of the solar cell dye N719 by acetonitrile, 3-methoxypropionitrile, and 4-tert-butylpyridine. *Sol. Energy Mater. Sol. Cells* **2007**, *91*, 1934–1942.
- (12) Abbotto, A.; Coluccini, C.; Dell'Orto, E.; Manfredi, N.; Trifiletti, V.; Salamone, M. M.; Ruffo, R.; Acciarri, M.; Colombo, A.; Dragonetti, C.; Ordanini, S.; Roberto, D.; Valore, A. Thiocyanate-free cyclometalated ruthenium sensitizers for solar cells based on heteroaromatic-substituted 2-arylpyridines. *Dalton Trans.* **2012**, *41*, 11731–11738.
- (13) Bomben, P. G.; Gordon, T. J.; Schott, E.; Berlinguette, C. P. A trisheteroleptic cyclometalated Ru^{II} sensitizer that enables high power output in a dye-sensitized solar cell. *Angew. Chem., Int. Ed.* **2011**, *50*, 10682–10685.
- (14) Bomben, P. G.; Koivisto, B. D.; Berlinguette, C. P. Cyclometalated Ru complexes of type $[Ru^{II}(N\wedge N)_2(C\wedge N)]^2-$: Physicochemical response to substituents installed on the anionic ligand. *Inorg. Chem.* **2010**, *49*, 4960–4971.
- (15) Bomben, P. G.; Thériault, K. D.; Berlinguette, C. P. Strategies for optimizing the performance of cyclometalated ruthenium sensitizers for dye-sensitized solar cells. *Eur. J. Inorg. Chem.* **2011**, *2011*, 1806–1814.
- (16) Bomben, P. G.; Borau-Garcia, J.; Berlinguette, C. P. Three is not a crowd-efficient sensitization of TiO₂ by a bulky trichromic trisheteroleptic cycloruthenated dye. *Chem. Commun.* **2012**, *48*, 5599–5601.
- (17) Polander, L. E.; Yella, A.; Curchod, B. F. E.; Astani, N. A.; Teucher, J.; Scopelliti, R.; Gao, P.; Mathew, S.; Moser, J.-E.; Tavernelli, I.; Rothlisberger, U.; Grätzel, M.; Nazeeruddin, M. K.; Frey, J. Towards compatibility between ruthenium sensitizers and cobalt electrolytes in dye-sensitized solar cells. *Angew. Chem., Int. Ed.* **2013**, *52*, 8731–8735.
- (18) Funaki, T.; Otsuka, H.; Onozawa-Komatsuzaki, N.; Kasuga, K.; Sayama, K.; Sugihara, H. Systematic evaluation of HOMO energy levels for efficient dye regeneration in dye-sensitized solar cells. *J. Mater. Chem. A* **2014**, *2*, 15945–15951.
- (19) Li, G.; Wu, S. J.; Wu, C. G. Structural design of ruthenium sensitizer compatible with cobalt electrolyte for a dye-sensitized solar cell. *J. Mater. Chem. A* **2014**, *2*, 17551–17560.
- (20) Frisch, M. J.; Trucks, G. W.; Schlegel, H. B.; Scuseria, G. E.; Robb, M. A.; Cheeseman, J. R.; Scalmani, G.; Barone, V.; Mennucci, B.; Petersson, G. A.; Nakatsuji, H.; Caricato, M.; Li, X.; Hratchian, H. P.; Izmaylov, A. F.; Bloino, J.; Zheng, G.; Sonnenberg, J. L.; Hada, M.; Ehara, M.; Toyota, K.; Fukuda, R.; Hasegawa, J.; Ishida, M.; Nakajima, T.; Honda, Y.; Kitao, O.; Nakai, H.; Vreven, T.; Montgomery, J. A., Jr.; Peralta, J. E.; Ogliaro, F.; Bearpark, M.; Heyd, J. J.; Brothers, E.; Kudin, K. N.; Staroverov, V. N.; Kobayashi, R.; Normand, J.; Raghavachari, K.; Rendell, A.; Burant, J. C.; Iyengar, S. S.; Tomasi, J.; Cossi, M.; Rega, N.; Millam, J. M.; Klene, M.; Knox, J. E.; Cross, J. B.; Bakken, V.; Adamo, C.; Jaramillo, J.; Gomperts, R.; Stratmann, R. E.; Yazyev, O.; Austin, A. J.; Cammi, R.; Pomelli, C.; Ochterski, J. W.; Martin, R. L.; Morokuma, K.; Zakrzewski, V. G.; Voth, G. A.; Salvador, P.; Dannenberg, J. J.; Dapprich, S.; Daniels, A. D.; Farkas, O.; Foresman, J. B.; Ortiz, J. V.; Cioslowski, J.; Fox, D. J. *Gaussian 09*, revision A.02; Gaussian, Inc.: Wallingford, CT, 2009.
- (21) Becke, A. D. Density-functional thermochemistry. III. The role of exact exchange. *J. Chem. Phys.* **1993**, *98*, 5648–5652.
- (22) Lee, C.; Yang, W.; Parr, R. G. Development of the Colle-Salvetti correlation-energy formula into a functional of the electron density. *Phys. Rev. B: Condens. Matter Mater. Phys.* **1988**, *37*, 785–789.
- (23) Hay, P. J.; Wadt, W. R. Ab initio effective core potentials for molecular calculations. Potentials for the transition metal atoms Sc to Hg. *J. Chem. Phys.* **1985**, *82*, 270–283.
- (24) McLean, A. D.; Chandler, G. S. Contracted Gaussian basis sets for molecular calculations. I. Second row atoms, Z = 11–18. *J. Chem. Phys.* **1980**, *72*, 5639–5648.
- (25) Cossi, M.; Rega, N.; Scalmani, G.; Barone, V. Energies, structures, and electronic properties of molecules in solution with the C-PCM solvation model. *J. Comput. Chem.* **2003**, *24*, 669–681.
- (26) Cossi, M.; Barone, V. Time-dependent density functional theory for molecules in liquid solutions. *J. Chem. Phys.* **2001**, *115*, 4708–4717.
- (27) Barone, V.; Cossi, M. Quantum calculation of molecular energies and energy gradients in solution by a conductor solvent model. *J. Phys. Chem. A* **1998**, *102*, 1995–2001.
- (28) Coluccini, C.; Manfredi, N.; Calderon, E. H.; Salamone, M. M.; Ruffo, R.; Roberto, D.; Lobello, M. G.; De Angelis, F.; Abbotto, A. Photophysical and electrochemical properties of thiophene-based 2-arylpyridines. *Eur. J. Org. Chem.* **2011**, *2011*, 5587–5598.
- (29) In fact, a racemate (meaning a mixture of two enantiomers; also called a racemic mixture) also cannot be distinguished by NMR spectroscopy. Typical laboratory purification methods (normal-phase, reversed-phase, and size-exclusion chromatography, recrystallization, distillation, extraction, etc.) cannot separate two enantiomers because of their same chemical and physical properties. Importantly, in an achiral environment such as a DSC cell, two enantiomers behave in the same way. Therefore, we support that the isolation of each enantiomer is really unnecessary in DSC.
- (30) Hartley, F. R. The *cis*- and *trans*-effects of ligands. *Chem. Soc. Rev.* **1973**, *2*, 163–179.
- (31) DUY2 and its ester form show a small δ difference ($\Delta\delta = 0.1$ ppm) of their two ortho protons, related to the ester-to-acid conversion, while two ortho protons of DUY4 and its ester form are almost the same ($\Delta\delta = 0.013$ ppm). This indicates that the ester-to-acid conversion of ligand Et₂dcby has not influenced the magnetic environment around the ortho protons of DUY4 and its ester form, or, in other words, Et₂dcby orients *trans* to the benzene ring and ligand B20 *trans* to the pyridine ring of the cyclometalating ligand.
- (32) Boschloo, G.; Gibson, E. A.; Hagfeldt, A. Photomodulated voltammetry of iodide/triiodide redox electrolytes and its relevance to dye-sensitized solar cells. *J. Phys. Chem. Lett.* **2011**, *2*, 3016–3020.
- (33) Chen, C. Y.; Pootrakulchote, N.; Chen, M. Y.; Moehl, T.; Tsai, H. H.; Zakeeruddin, S. M.; Wu, C. G.; Grätzel, M. A new heteroleptic ruthenium sensitizer for transparent dye-sensitized solar cells. *Adv. Energy Mater.* **2012**, *2*, 1503–1509.

(34) Wang, Q.; Moser, J. E.; Grätzel, M. Electrochemical impedance spectroscopic analysis of dye-sensitized solar cells. *J. Phys. Chem. B* **2005**, *109*, 14945–14953.

(35) Bisquert, J.; Fabregat-Santiago, F.; Mora-Seró, I.; Garcia-Belmonte, G.; Giménez, S. Electron lifetime in dye-sensitized solar cells: Theory and interpretation of measurements. *J. Phys. Chem. C* **2009**, *113*, 17278–17290.

(36) Merhi, A.; Zhang, X.; Yao, D.; Drouet, S.; Mongin, O.; Paul, F.; Williams, J. A. G.; Fox, M. A.; Paul-Roth, C. O. New donor–acceptor conjugates based on a trifluorenylporphyrin linked to a redox-switchable ruthenium unit. *Dalton Trans.* **2015**, *44*, 9470–9485.

(37) Simon, S. J. C.; Parlane, F. G. L.; Swords, W. B.; Kellett, C. W.; Du, C.; Lam, B.; Dean, R. K.; Hu, K.; Meyer, G. J.; Berlinguette, C. P. Halogen bonding promotes higher dye-sensitized solar cell photovoltages. *J. Am. Chem. Soc.* **2016**, *138*, 10406–10409.

(38) Clifford, J. N.; Palomares, E.; Nazeeruddin, M. K.; Grätzel, M.; Durrant, J. R. Dye dependent regeneration dynamics in dye sensitized nanocrystalline solar cells: evidence for the formation of a ruthenium bipyridyl cation/iodide intermediate. *J. Phys. Chem. C* **2007**, *111*, 6561–6567.